Ten Interventional Oncology Pitfalls

Lessons learned from complications encountered during interventional oncology procedures.

BY NICHOLAS FIDELMAN, MD; MATTHEW D. BUCKNOR, MD; PAUL HASTE, MD; MAUREEN P. KOHI, MD; RYAN M. KOHLBRENNER, MD; K. PALLAV KOLLI, MD; KRISTEN LEE, MD; EVAN D. LEHRMAN, MD; THOMAS M. LINK, MD, PHD; AND ANDREW G. TAYLOR, MD, PHD

1. HEPATIC ARTERY DISSECTIONS HEAL OVER TIME

A 68-year-old woman with chemotherapy-refractory colon cancer that had metastasized to the liver developed a common hepatic artery dissection (Figures 1A and 1B) during mapping hepatic arteriography performed in preparation for yttrium-90 radioembolization. Repeat conventional and CTA performed 2 months later demonstrated improvement in hepatic artery flow (Figures 1C and 1D).

Hepatic artery dissection is a rare complication of angiography. Dissection can occur when catheters and wires are advanced too forcefully within hepatic vessels, but it is much more likely to occur in the friable arteries found in patients undergoing treatment with antiangiogenesis drugs such as bevacizumab.[1] This complication may limit the ability to deliver arterial cancer therapies. Although the instinct of the interventional radiologist may be to perform maneuvers to fix the dissection, often the best course of action is to terminate the procedure. Attempting angioplasty or stenting to tack down the intimal flap has the potential to propagate the dissection. Frequently, a common hepatic artery

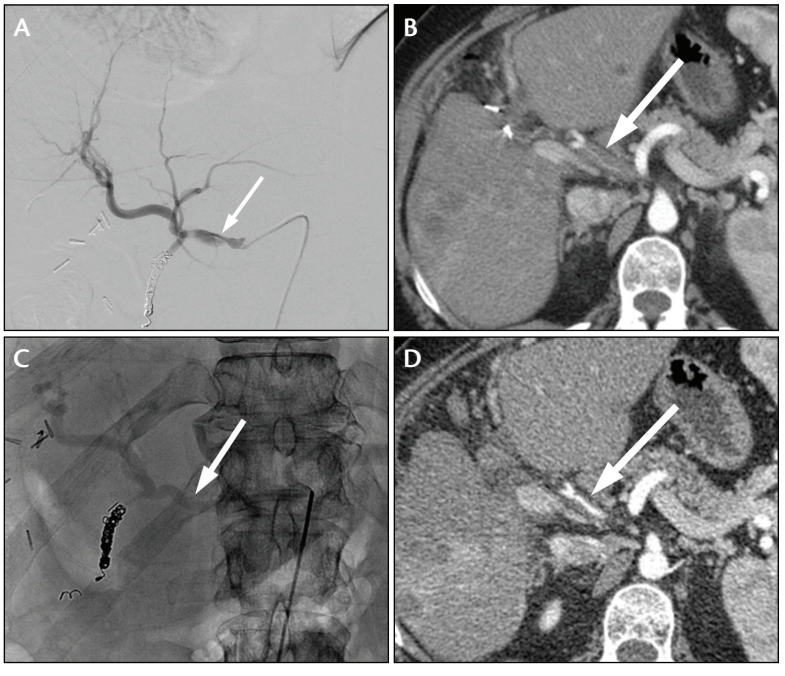

Figure 1. Common hepatic arteriography showed a flow-limiting dissection flap in the common hepatic artery. The GDA had been coiled in preparation for yttrium-90 radioembolization (A). CT performed 2 weeks after the dissection occurred showed a tiny channel of contrast running through concentrically thickened layers of thrombus in the false lumen of the dissected artery (B). Angiography performed 2 months after the dissection occurred showed a widely patent lumen with brisk antegrade flow, allowing for uneventful delivery of radioembolization spheres (C). Corresponding CT showed resorption of the thrombus with restoration of the patent true lumen back to predissection caliber (D).

dissection will heal over time, allowing for radioembolization or chemoembolization to be performed at a later date. If this does not happen, access to the hepatic artery from the superior mesenteric artery through the pancreaticoduodenal arcades—which have the tendency to hypertrophy because of the hypoxic insult of the dissection—to the gastroduodenal artery (GDA) may be obtained in patients who have not undergone GDA coiling.

2. TREAD LIGHTLY AFTER ARTERY DISSECTION

A 53-year-old patient with a well-differentiated pancreatic neuroendocrine tumor (NET) that had metastasized to the liver presented for preradioembolization mapping angiography. Previous planning angiography was aborted due to dissection of the celiac artery with extension to the common and proper hepatic arteries (Figure 2A). Four months later, hepatic artery flow had improved (Figure 2B). However, during attempted catheterization and embolization of the right gastric artery via the left gastric artery, the dissection was further propagated into the replaced left hepatic and right hepatic arteries (Figures 2C and 2D), which precluded radioembolization. This case demonstrates that dissection may propagate with repeat arterial catheterization. Instrumentation of previously dissected arteries should be kept to a minimum.

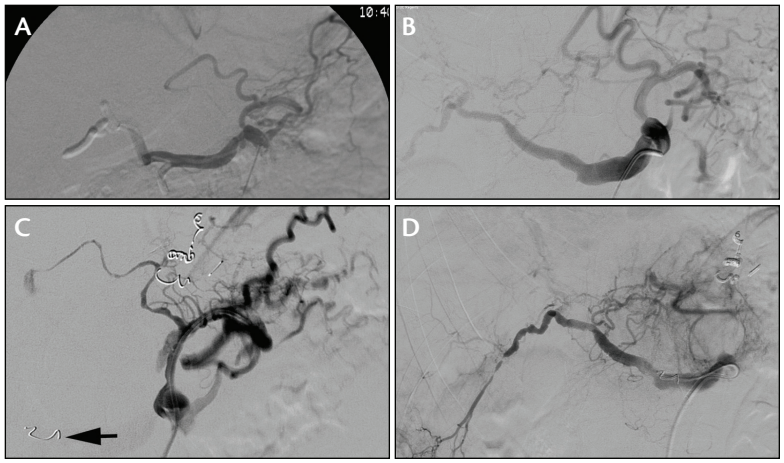

Figure 2. Preradioembolization mapping angiogram demonstrated dissection of the celiac artery with extension into the common and proper hepatic arteries (A). Repeat angiogram 4 months later demonstrated improved hepatic arterial perfusion (B). The dissection was propagated to the replaced left hepatic artery (C) and into the right hepatic artery (D) during catheterization and coil embolization (arrow) of the right gastric artery via the left gastric artery.

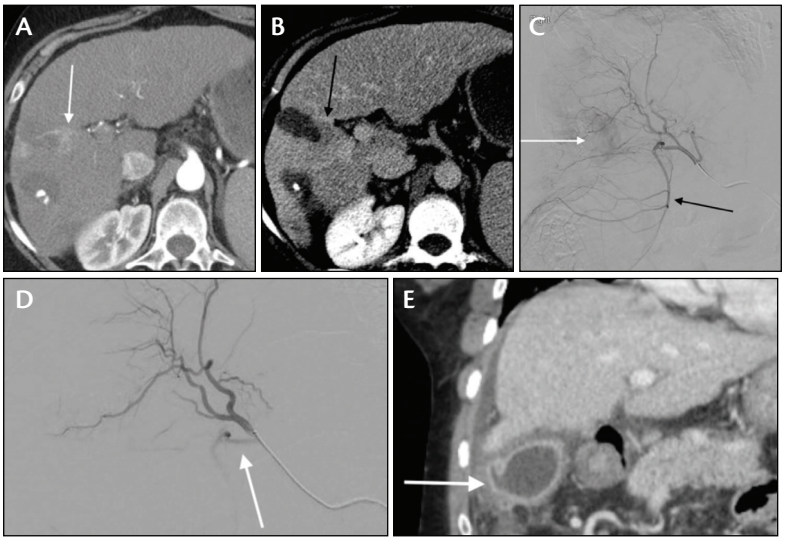

Figure 3. Contract-enhanced CT demonstrated hypervascularity on arterial phase (A) and corresponding washout on a delayed phase (B) adjacent to a region of prior treatment, consistent with recurrent HCC. The hepatic arteriogram demonstrated hypervascularity characteristic of recurrent HCC. Note the large cystic artery (C, arrow). The angiogram of the right hepatic artery prior to TACE showed reflux into the cystic artery (D, arrow). CT obtained 3 weeks after TACE demonstrated gallbladder wall thickening with perforation (E, arrow).

3. DISASTROUS REFLUX DURING EMBOLIZATION

A 60-year-old woman with cirrhosis due to hepatitis C and hepatocellular carcinoma (HCC) was treated with thermal ablation and multiple chemoembolizations. Follow-up contrast-enhanced CT showed recurrent HCC (Figures 3A and 3B). Arteriography demonstrated hypervascular tumor blush in the right lobe (Figure 3C). Transarterial chemoembolization (TACE) was performed by administering 100–300-µm LC Beads (BTG International) loaded with doxorubicin into the right hepatic artery (Figure 3D). The patient presented to the emergency department 3 weeks after the TACE procedure with clinical symptoms of cholecystitis, which was confirmed on CT (Figure 3E). A cholecystectomy was performed, and the gallbladder was found to be inflamed and perforated. In retrospect, reflux of microspheres into the cystic artery must have occurred (Figure 3D).

4. REAL DANGER OF PSEUDOCIRRHOSIS

A 55-year-old woman with chemorefractory metastatic breast cancer to the liver presented for TACE. Preprocedure positron emission tomography (PET)/CT demonstrated numerous hypermetabolic lesions throughout the liver (Figure 4A) and pseudocirrhosis (Figure 4B). The patient's total bilirubin level was normal at the time of TACE. The common hepatic angiogram showed multiple hypovascular lesions in the right hepatic lobe (Figure 4C). The patient underwent lobar TACE using one vial of 70–150-µm LC Beads loaded with 75 mg of doxorubicin. After the TACE procedure, the patient experienced postembolization syndrome and transaminitis. Follow-up CT 3 weeks later demonstrated worsening liver pseudocirrhosis and new-onset ascites (Figure 4D). The patient was then hospitalized, received supportive care, and died from liver failure within 2 months of the TACE procedure.

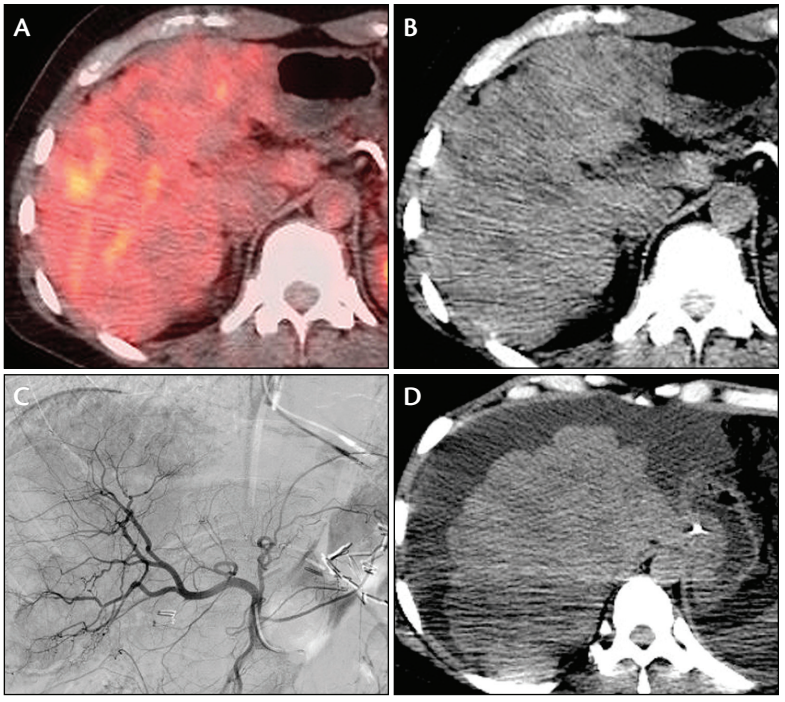

Figure 4. Fused PET/CT (A) and CT (B) images demonstrated multiple PET-avid liver metastases in the background of nodular liver due to pseudocirrhosis. The angiogram showed multiple large hypervascular masses in the right liver lobe (C). Follow-up CT obtained 3 weeks after TACE demonstrated new-onset ascites (D).

Pseudocirrhosis refers to the morphologic changes in the liver due to chemotherapy for metastatic disease and resembles macronodular cirrhosis on imaging.[2] Although the underlying etiology is unclear, patients with pseudocirrhosis can progress to liver failure, particularly following anticancer therapy.[2] Hepatotoxicity after TACE is common in patients with liver metastases from breast cancer.[3,4] Therefore, TACE should be performed with caution in the setting of liver metastases from breast cancer and pseudocirrhosis, even when baseline liver function tests are relatively normal.

5. TACKLING CARCINOID CRISIS

A 59-year-old man with a history of metastatic well-differentiated NET of the ileum (carcinoid) and multiple, slow-growing, diffuse liver metastases (Figure 5) despite ongoing therapy with a somatostatin analogue was referred for transarterial embolotherapy. At the time of the referral, the patient had debilitating carcinoid syndrome symptoms, which included cutaneous flushing multiple times per day and diarrhea (up to 10 bowel movements/day). Due to diffuse and multifocal distribution of liver metastases, selective internal radiation therapy with yttrium-90 microspheres was selected. The patient developed severe erythema involving the head, neck, and upper torso; hypertension; and severe abdominal and lower back cramps within minutes of a proper hepatic angiography using nonionic iso-osmolar contrast at a rate of 4 mL/s for 20 mL. The procedure was aborted because of the patient's inability to remain in the supine position. All symptoms abated 1 hour after administration of intravenous octreotide.

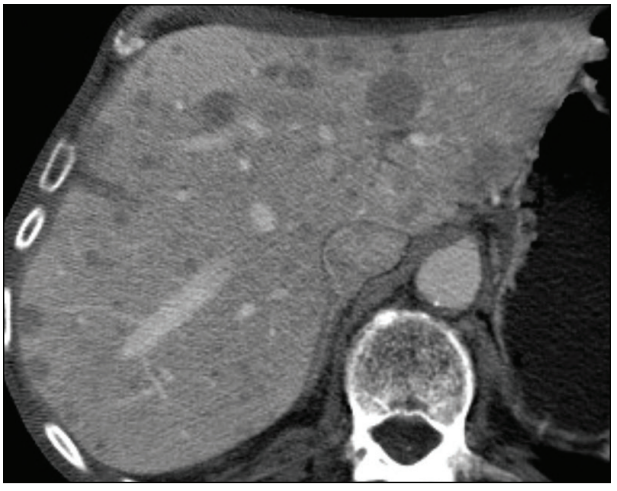

Figure 5. Contrast-enhanced CT obtained prior to radioembolization demonstrated multiple bilobar liver lesions.

This case describes carcinoid storm, which occurred in the setting of hepatic angiography in a patient with known carcinoid syndrome. Symptoms of carcinoid storm may include severe cutaneous flushing, abdominal cramps, diarrhea, facial swelling, as well as labile blood pressure and heart rate. Patients with a history of carcinoid syndrome and even asymptomatic patients with metastatic well-differentiated NETs of bowel and bronchial origin are at risk of developing carcinoid crisis during manipulation of the liver tumors, which includes intraoperative liver mobilization, hepatic angiography, and hepatic embolization.

The risk of carcinoid crisis may be reduced with preprocedural and intraprocedural administration of a somatostatin analogue (octreotide 150 µg/h intravenously and octreotide 150 µg every 8 hours subcutaneously), hydration, and H_1 and H_2 receptor blockers, such as diphenhydramine and famotidine. Intravenous β-blockers (ie, labetalol) may be useful for treatment of hypertension. Epinephrine should be avoided, as it may exacerbate carcinoid crisis.[5]

6. POSTABLATION NONCONTRAST IMAGES COUNT

A 75-year-old man with renal cell carcinoma (Figure 6A) was treated with cryoablation. On follow-up imaging 1 year after cryoablation, the reporting radiologist raised suspicion for recurrence based on postcontrast images (Figure 6B), but after review of noncontrast images, it was determined to be calcification (Figure 6C). Inflammatory changes and dystrophic calcifications are common after thermal ablation. It is imperative that noncontrast images be obtained prior to administering intravenous contrast for any surveillance study after ablation of kidney masses to reduce false-positive diagnoses of tumor recurrence.

7. DANGER AT THE BODY-WALL BOUNDARY

A 58-year-old man with a 3-cm solid left upper pole renal mass was referred for thermal ablation. The mass was considered favorable for ablation given its posterior

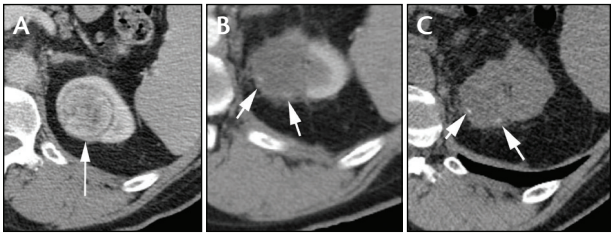

Figure 6. Contrast-enhanced CT demonstrated a solid right renal mass (A). One year after cryoablation, tumor recurrence was suggested by the interpreting radiologist (B, arrows); however, review of the corresponding noncontrast CT image (C) showed that the hyperdensity was due to dystrophic calcifications rather than enhancing tumor.

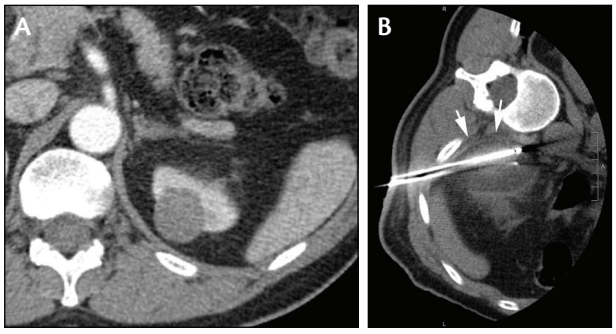

Figure 7. Axial postcontrast CT image demonstrated a hypoenhancing left renal mass suspicious for renal cell carcinoma, which was in close proximity to the left 12th rib (A). Axial noncontrast CT image obtained in the left lateral decubitus position during percutaneous cryoablation showed that the ice ball margin (arrows) extended into the body wall and abutted the 12th rib (B).

location and exophytic nature (Figure 7A). The patient underwent a technically successful cryoablation with three cryoprobes. During the second of two freeze cycles, the ice ball approached the body wall adjacent to the 12th rib (Figure 7B). One week after ablation, the patient developed left lower abdominal wall laxity and a pins and needles sensation in the left T12 distribution, which was compatible with intercostal nerve palsy.

Because posterior renal masses may share a boundary with the body wall, protective measures such as hydrodissection, pneumodissection, or balloon displacement may be considered to protect thoracolumbar nerve roots and intercostal nerves. Although symptoms from nerve injuries sustained during ablation are usually self-limited, symptoms may persist for several months. Patients with severe symptoms may benefit from gabapentin, which is commonly prescribed for diabetic neuropathy and other neuropathic pain.

8. ADRENAL ABLATION'S ADRENALINE RUSH

A 62-year-old man with a history of cirrhosis and multifocal HCC developed a solitary HCC metastasis in the right adrenal gland 3 years after orthotopic liver transplantation (Figure 8A). The lesion was biopsied and treated with percutaneous radiofrequency ablation during the same session (Figure 8B). The patient experienced sharp elevations in blood pressure (systolic pressure up to 290–300 mm Hg) toward the end of energy application. The anesthesiologist rapidly treated blood pressure spikes with no adverse clinical sequelae.

Local tumor recurrence was detected in the right adrenal gland 10 months later (Figure 8C). The patient was evaluated by an endocrinologist and pretreated with 10 mg of phenoxybenzamine daily for 2 weeks before percutane-

ous cryoablation (Figure 8D). Real-time intraprocedural hemodynamic monitoring via an arterial line was employed during cryoablation. During the procedure, only mild elevations in blood pressure (systolic blood pressure up to 180 mm Hg) were noted during thaw cycles. This case illustrates the importance of periprocedural α-adrenergic blockade when performing thermal ablation of adrenal masses.[6]

9. MISSING INVISIBLE MARGINS

A 46-year-old man presented with occipital cervical leiomyosarcoma, which was initially treated with resection followed by chemotherapy and radiation. Over the subsequent 8-year period, distant metastases developed, which were treated with additional chemotherapy, pulmonary wedge resection, pancreatectomy, splenectomy, and partial left nephrectomy. Eight years after initial diagnosis, the patient developed a 9-mm solitary metastasis in the right ischium (Figure 9A). The patient requested radiofrequency ablation of the solitary bone metastasis.

Using CT guidance, a Bonopty (AprioMed, Inc.) access needle and drill device were used to place a 16-gauge, 1-cm active tip radiofrequency ablation probe at the center of the lesion with the patient in supine position and under general anesthesia. Per standard procedure,

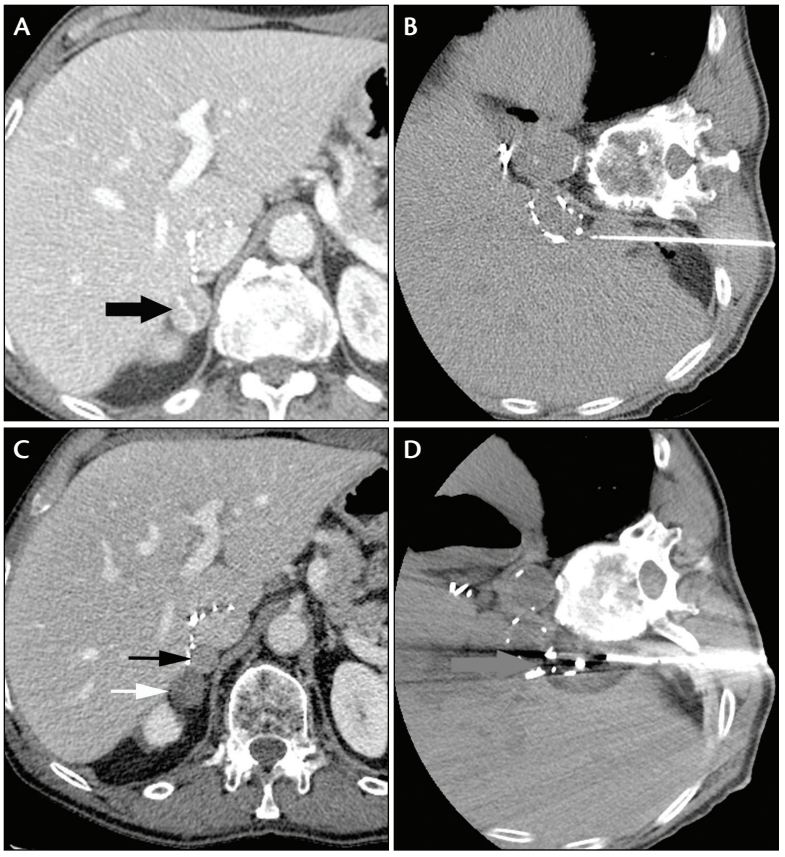

Figure 8. Contrast-enhanced CT axial image demonstrated enhancing right adrenal mass (A, arrow), which was subsequently confirmed as metastatic HCC with percutaneous biopsy. The radiofrequency ablation probe was positioned within the metastasis (B). Contrast-enhanced CT image obtained 10 months after radiofrequency ablation demonstrated a recurrent right adrenal mass (C), which was treated with percutaneous cryoablation (D).

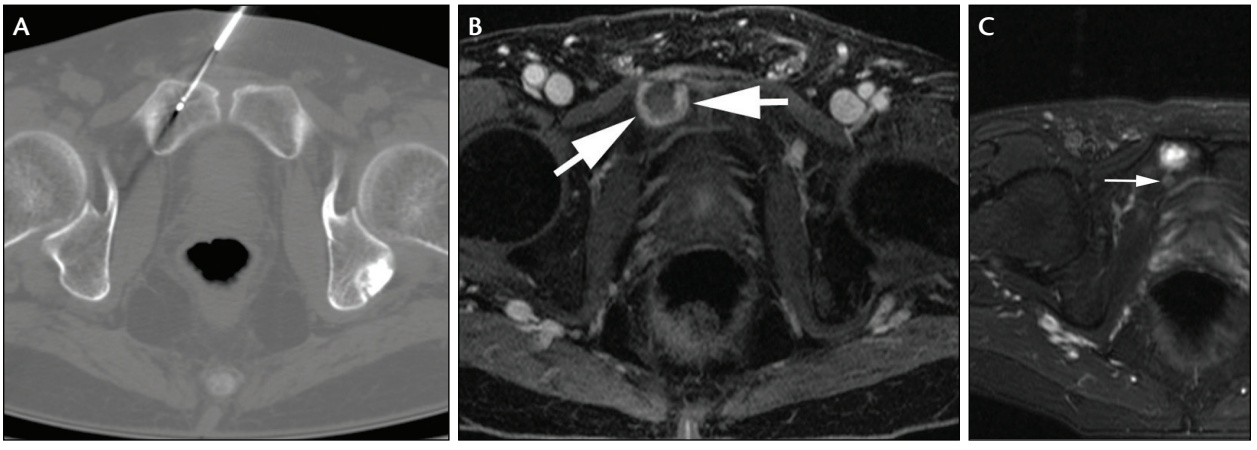

Figure 9. Placement of a radiofrequency ablation probe in radiolucent metastasis under CT guidance (A). A thick rim of enhancement (arrow) on T1-weighted fat-saturated postcontrast MRI obtained 1 month after radiofrequency ablation was consistent with focal bone marrow necrosis (B). A small satellite metastasis (arrow) in the vicinity of the treated lesion was detected 6 months after radiofrequency ablation (C).

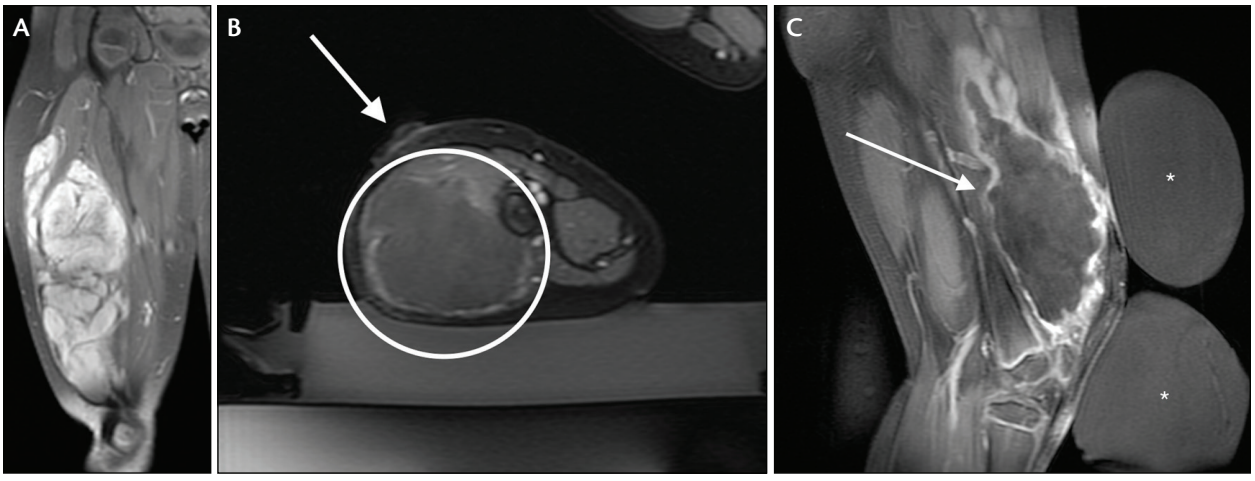

Figure 10. Coronal spoiled gradient echo fat-saturated postcontrast image before first MRgFUS treatment demonstrated large desmoid tumor within the posterior musculature of the thigh (A). Axial spoiled gradient echo fat-saturated postcontrast image obtained immediately after the first MRgFUS treatment. A large area of nonperfusion was seen centrally within the mass (white circle). However, there was an associated third-degree skin burn at the far-field air-skin interface with an associated skin blister demonstrated in this region (white arrow) (B). Sagittal spoiled gradient echo fat-saturated postcontrast image obtained immediately after fifth MRgFUS treatment. A large area of nonperfusion was seen centrally within the mass (white arrow). Water bags (asterisks) were used in subsequent treatments along the far-field skin to provide direct skin cooling and act as an acoustic conduit (C).

a 7-minute ablation cycle with a final temperature of 95° C was performed. One month after ablation, surveillance imaging demonstrated a thick rim of enhancing tissue around the ablation cavity, which had the typical morphology for focal bone marrow necrosis (Figure 9B). However, the patient developed a small satellite metastasis near the tumor after 6 months, suggesting that viable tumor tissue was left behind (Figure 9C).

Thermal ablation is an acceptable approach for the treatment of oligometastatic disease to the skeleton. Focal treatment prevents or delays the systemic toxicity that accompanies chemotherapy but should be reserved for patients with a chance for a cure. The largest published study on this topic described a local control rate of at least 87% to 97%.[7] Local recurrences may nevertheless be encountered after radiofrequency ablation. In this case, the tumor may have been resistant to radiofrequency ablation with tumor cells surviving the standard radiofrequency ablation cycle. A longer ablation that included a larger area would have potentially provided better local tumor control.

10. BLISTERS AFTER HIGH-INTENSITY FOCUSED ULTRASOUND

A 7-year-old boy presented with a recurrent desmoid tumor within the right thigh. The tumor had previously been treated with surgical resection, intraoperative radiation, chemotherapy, and sorafenib. The patient was referred for magnetic resonance-guided focused ultrasound (MRgFUS) ablation. Pretreatment tumor volume was approximately 770 cm^3 (Figure 10A). The treatment was performed with 96 sonications, with energy ranging from 1,400 to 3,000 J per sonication. There was approximately 75% nonenhancing volume after the initial treatment. However, treatment was complicated by a third-degree skin burn that occurred along the far-field air-skin interface, not at the near-field skin entry site where sound energy entered the patient, which was likely secondary to reflection of sound energy back into the skin and the superficial subcutaneous tissues (Figure 10B). Magnetic resonance thermometry, which creates images of interval differences in temperature, did not detect the gradual significant heat accumulation in this region over the course of the treatment. The burn healed with conservative measures. The patient had four additional MRgFUS treatments, during which chilled water bags were placed along the far-field skin to serve as an acoustic conduit and protect the skin (Figure 10C).[8] ■

1. Brown DB. Hepatic artery dissection in a patient on bevacizumab resulting in pseudoaneurysm formation. Semin Intervent Radiol. 2011;28:142-146.
2. Zeina AR, Abu-Mouch S, Mari A. Pseudocirrhosis in metastatic breast cancer. Isr Med Assoc J. 2017;19:328.
3. Lin YT, Médioni J, Amouyal G, et al. Doxorubicin-loaded 70-150 µm microspheres for liver-dominant metastatic breast cancer: results and outcomes of a pilot study. Cardiovasc Intervent Radiol. 2017;40:81-89.
4. Martin RC, Robbins K, Fagès JF, et al. Optimal outcomes for liver-dominant metastatic breast cancer with transarterial chemoembolization with drug-eluting beads loaded with doxorubicin. Breast Cancer Res Treat. 2012;132:753-763.
5. Kunz PL, Redy-Lagunes D, Anthony LB, et al. Consensus guidelines for the management and treatment of neuroendocrine tumors. Pancreas. 2013;42:557-577.
6. Espinosa De Ycaza EA, Welch TL, Ospina NS, et al. Image-guided thermal ablation of adrenal metastases: hemodynamic and endocrine outcomes. Endocr Pract. 2017;23:132-140.
7. Kurup AN, Callstrom MR. Expanding role of percutaneous ablative and consolidative treatments for musculoskeletal tumors. Clinical Radiol. 2017;72:645-656.
8. Bucknor MD, Rieke V. MRgFUS for desmoid tumors within the thigh: early clinical experiences. J Ther Ultrasound. 2017;5:4.

Nicholas Fidelman, MD
Department of Radiology and Biomedical Imaging
University of California San Francisco
San Francisco, California
nicholas.fidelman@ucsf.edu
Disclosures: Research grant from Sirtex Medical, Inc.

Matthew D. Bucknor, MD
Department of Radiology and Biomedical Imaging
University of California San Francisco
San Francisco, California
Disclosures: None.

Paul Haste, MD
Department of Radiology and Biomedical Imaging
University of California San Francisco
San Francisco, California
Disclosures: None.

Maureen P. Kohi, MD
Department of Radiology and Biomedical Imaging
University of California San Francisco
San Francisco, California
Disclosures: None.

Ryan M. Kohlbrenner, MD
Department of Radiology and Biomedical Imaging
University of California San Francisco
San Francisco, California
Disclosures: None.

K. Pallav Kolli, MD
Department of Radiology and Biomedical Imaging
University of California San Francisco
San Francisco, California
Disclosures: None.

Kristen Lee, MD
Department of Radiology and Biomedical Imaging
University of California San Francisco
San Francisco, California
Disclosures: None.

Evan D. Lehrman, MD
Department of Radiology and Biomedical Imaging
University of California San Francisco
San Francisco, California
Disclosures: None.

Thomas M. Link, MD, PhD
Department of Radiology and Biomedical Imaging
University of California San Francisco
San Francisco, California
Disclosures: None.

Andrew G. Taylor, MD, PhD
Department of Radiology and Biomedical Imaging
University of California San Francisco
San Francisco, California
Disclosures: None.